ChemElectroChem

Research Article
doi.org/10.1002/celc.202200474

Chemistry Europe
European Chemical Societies Publishing

www.chemelectrochem.org

A Multi-Functional Separator for Li-S Batteries: WS_2@C Nanoflowers Catalyze the Rapid Recycling of Lithium Polysulfides by Polar Attraction

Fanxuan Xie[+],[a] Man Xiong[+],[a] Jiapeng Liu,[a] Jingwen Qian,*[a, b] Tao Mei,[a] Jinghua Li,[a] Jianyin Wang,[a] Li Yu,[a] Jan P. Hofmann,[b] and Xianbao Wang*[a]

Featuring high theoretical capacity, environmental friendliness and low cost, lithium-sulfur (Li-S) batteries become promising alternatives to satisfy the growing demand for energy storage. To boost their energy density for practical application, modified separators are needed to suppress shuttle effects resulting from the solubility of lithium polysulfides (LiPSs). Herein, we modified traditional polypropylene (PP) separators with functional WS_2@C nanoflower composites (WS_2@C-PP). They can effectively adsorb LiPSs and catalyze their conversion on the edge sites of the WS_2. Also, the unique construction of a carbon layer coating on the WS_2 nanoflowers combines active sites and conducting properties. The material benefits the reversibility of redox reactions and reutilization of active materials. With the WS_2@C-PP separator, the cell displays improved cycling stability and rate performance. When cycling at 0.1 C, the cell discharges a capacity of up to 1475 mAh g^{-1}, and it contributes 943 mAh g^{-1} originally at 1 C, with a decay rate of only 0.07% after 500 cycles. Our work highlights the potential of functional separators to advance the properties of Li-S batteries.

Introduction

The need of using renewable energy sources for making the transition to a future, CO_2-neutral energy system comes along with the requirement for efficient energy storage systems, where batteries will play an indispensable role. From portable electronics, like smartphones, to electrical vehicles and grids, batteries are present everywhere in our daily life.[1] As the energy density of lithium-ion batteries cannot meet the increasing practical application requirements in, for instance, all-electric vehicles and grid-scale energy storage applications,[2,3] it is imperative to develop alternative battery concepts.[4] Notably, lithium-sulfur (Li-S) batteries arouse wide interest owing to their low cost, environmental friendliness, and ultrahigh theoretical capacity of as high as 1675 mAh g^{-1}. Moreover, the specific energy density of Li-S batteries (2600 Wh kg^{-1}) is up to five times higher than that of current Li-ion batteries.[5–7]

However, one of the critical shortcomings of Li-S batteries is the so-called shuttle effect. Specifically, soluble intermediates of the redox reactions between the Li_2S and elemental S would directly react with lithium to cause irreversible loss of active materials, leading to fast capacity decay, low coulombic efficiency, and large internal resistance.[8,9] Those severely hinder the commercial implementation of Li-S batteries. Also, inhomogeneous deposition on the anode surface may lead to 'dead' lithium and unstable electrode-electrolyte interphase, which will result in further polarization.[10–12] Based on fundamental understanding, numerous efforts have been dedicated to fabricating various sulfur host materials or modifying anodes. For instance, carbon-based materials,[13–15] conductive polymers,[16] and graphene[17] are commonly employed as cathodes. Meanwhile, utilizing lithiophilic matrices[18,19] and protective interface layers[20,21] are the usual ways to modify anodes. These methods are limited by their complex synthetic requirements, and the inert host materials would decrease the energy density.[22] Thus, it is necessary to design novel strategies to suppress shuttle effects as well as to ensure an ideal sulfur content of the cathodes by decreasing the share of inactive materials. A possible route to achieving this is the use of functional separators. As an indispensable part of the battery, separators contact and interact with both electrodes, preventing internal short circuits while providing transport pathways for ions.[23–25] Initially, various carbon-based materials with controlled pore size are made as free-standing interlayer/

[a] F. Xie,[+] M. Xiong,[+] J. Liu, Dr. J. Qian, Prof. T. Mei, Prof. J. Li, Prof. J. Wang, Prof. L. Yu, Prof. X. Wang
Hubei Collaborative Innovation Center for Advanced Organic Chemical Materials
Ministry-of-Education Key Laboratory for the Green Preparation and Application of Functional Materials
Hubei Key Laboratory of Polymer Materials (Hubei University)
School of Materials Science and Engineering
Hubei University
430062 Wuhan, PR China
E-mail: jqian@surface.tu-darmstadt.de
wxb@hubu.edu.cn
[b] Dr. J. Qian, Prof. J. P. Hofmann
Surface Science Laboratory
Department of Materials and Earth Sciences
Technical University of Darmstadt, Otto-Berndt-Strasse 3
64287 Darmstadt, Germany
[+] These authors contributed equally to this work.

Supporting information for this article is available on the WWW under https://doi.org/10.1002/celc.202200474

coating layer of separators.[2,26] Compared with conventional polypropylene (PP) and polyethylene (PE) separators, they can enhance the ionic conductivity and cover the bare mesoporous structure against lithium polysulfides (LiPSs) diffusion.[25] However, with the weak Van der Waals' forces, these materials could only provide feebly physical adsorption to polar LiPSs. In recent years, numerous works have researched the strong interaction of separators with LiPSs like electrostatic interaction[27] or chemical bonding[28,29,12] to alleviate shuttle effects. Huang's group, for instance, fabricated a Nafion-based membrane layer as the ion-selective membrane,[30] offering an electrostatic shield to LiPSs by SO_3^{2-} on the surfaces of the coating layers, while allowing Li^+ ion hopping. Meanwhile, Pei et al. reported an advanced separator consisting of nitrogen-doped carbon nanosheets supported on a PP separator.[31] Because the doped-N in the carbon matrix could boost polysulfide-binding via chemisorption, the battery exhibited better electrochemical performance. However, due to the limited function of ionic sieve caused by the LiPSs' high concentration, and the weak chemical binding of doped atoms as well as the uneven distribution of them into the matrix,[25] there is still much room for improvement for the above methods.

Nowadays, transition metal compounds have attracted large interest for their intrinsic polar surfaces and catalytic properties. Among them, transition metal (TM) sulfides (TMS), especially tungsten disulfides (WS_2) with unique physical and electrochemical properties,[32,33] have shown moderate adsorption to LiPSs through S-TM bonds formed by electrostatic interaction.[34,35] Hence, except for being applied as the S host materials,[36,37] they own a huge potential as functional separators, which could trap LiPSs on the sulfophilic sites instead of allowing diffusion to the anode side. However, it is not enough to just provide a strong affinity to LiPSs. Scientists have been exploring appropriate catalysts to promote the transformation of LiPSs, as the slow rate under high sulfur loading may lead to their serious accumulation in the electrolyte causing notorious shuttle effects.[38] Consequently, with the good conductivity, superb adsorptive ability towards LiPSs, and high catalytic activity for the relevant redox reactions, WS_2 is a prominent candidate and has not been explored thoroughly in Li-S batteries yet.[39,40] Moreover, due to the edge selectivity of catalytic sites cooperating with the distinct open-layered structure, WS_2 could provide plentiful active sites to promote the conversion reactions from long-chain to short-chain LiPSs as well as the deposition of Li_2S.[40,41]

Various carbonaceous materials have been compounded with WS_2 to promote electron conductivity and ion accessibility, furthering the electrochemical performances.[42–44] Ali et al. designed a bi-layer separator by mechanically mixing commercial carbon and WS_2 to alleviate the shuttle effects of LiPSs,[45] further benefiting rate performance and cycling stability. However, commercial bulk WS_2 contains only a small number of exposed edge sites, and physical blends of these polar materials and carbon cannot realize uniform, close contact between them. It is thus an advisable strategy to coat carbon on the surfaces of WS_2 by heat treatment to give full play to their synergism as well as ensure structural stability.[46] Additionally, resulting from the high surface energy and strong interlayer π-π interaction,[47,48] WS_2 nanosheets face inherent layer stacking and are kinetically favored to aggregate,[12] thus would decrease the number of exposed active sites and limit the conductivity through two stacked S–W–S interlayers.[47,49,50] In theory and practice, carbon coating could also act as a spacer[51] to solve the above problem and limit the growth of bulk WS_2,[52] finally forming the compound with homogeneous dispersions. Moreover, the nanosized carbon layer possessing large surface areas and rich porous structure, can block LiPSs physically and increase the wettability of electrolytes.[53]

In the present study, we fabricated simple and effective separators by modifying commercial PP separators with spherical WS_2@C composites (WS_2@C-PP). The special structure is derived from the flower-like WS_2 nanospheres composed of 2D nanosheets which are subsequently coated by carbon. This unique design owns several merits: (1) The WS_2 nanoflowers can provide abundant adsorptive/catalytic edge sites to anchor the LiPSs as well as to facilitate their conversion thereby ameliorating their accumulation. (2) Carbon-coated nanospheres could accelerate electron transfer to decrease the polarization of the relevant redox reactions and impede LiPSs' diffusion physically. Because of the large interlayer spacing and weak van der Waals interaction of WS_2,[30] the WS_2@C-PP materials hold preferential conduction pathways for electrons and diffusion pathways for ions, benefiting the reversibility of redox reactions and promoting the reutilization of LiPSs.[3,54] (3) The porous carbon-coated layer may inhibit the aggregation of WS_2 and construct robust nanostructures with improved mechanical strength,[55] obtaining uniform and stable WS_2@C layers on PP separators. Also, their special morphology makes the most combinations of polar materials and conductors to achieve the favorable synergism. This approach could reduce the wastage of active materials during the extra process from the adsorption sites to redox-active sites.[56] Profiting from the above-mentioned advantages, the WS_2@C-PP separators reveal superior electrochemical performances with a high initial discharge capacity and a stable capacity during long cycling, providing a facile and viable method to boost the development of the industrial fabrication and implementation for commercial Li-S batteries.

Results and Discussion

Materials Characterization

To construct a modified separator for Li-S batteries, we fabricated a multi-functional coated layer providing chemically adsorptive and electrocatalytic sites for LiPSs. In the preparation of the WS_2@C-PP composite (Figure 1), flower-like WS_2 nanospheres were synthesized from WCl_6 and C_2H_5NS via a hydrothermal method. Then, with polydopamine as carbon source, the as-prepared WS_2 nanospheres were annealed to carbonize in an argon atmosphere to form the WS_2@C composite. At last, the bi-layer composite was pasted onto a traditional PP separator to obtain the WS_2@C-PP separator. Further details on

Research Article
doi.org/10.1002/celc.202200474
Chemistry Europe
European Chemical Societies Publishing

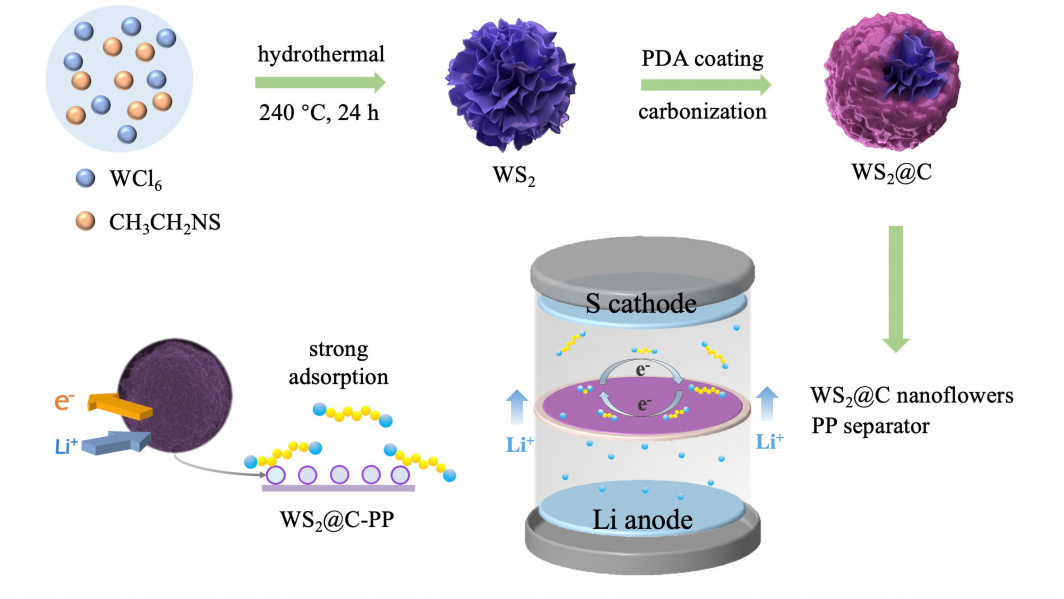

Figure 1. Schematic illustration of the fabrication of WS_2@C composite and its working mechanism in Li-S battery.

the experimental procedures can be found in the Experimental Section.

The microstructure and morphology were characterized by field emission scanning electron microscopy (FESEM). From Figure 2a, we can see that the as-prepared WS_2 shows the

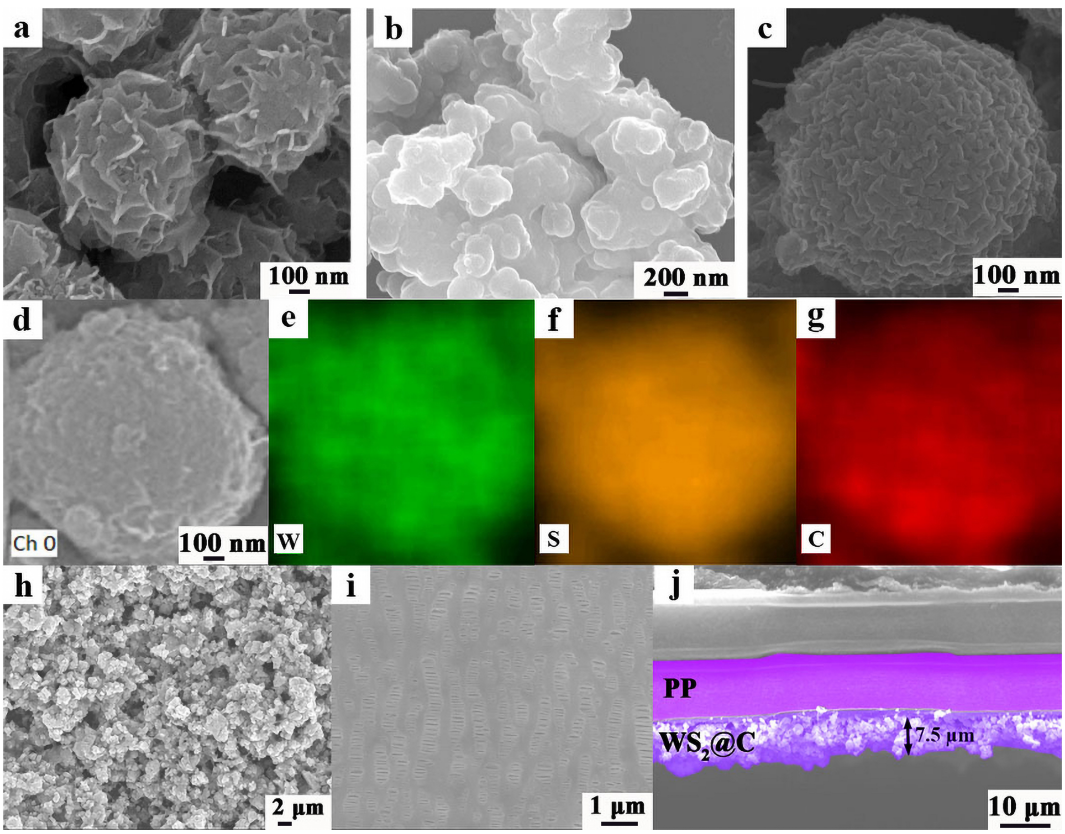

Figure 2. (a) FESEM image of WS_2. (b, c) FESEM images of WS_2@C with various resolutions. (d) FESEM image of WS_2@C and EDX elemental maps of (e) W, (f) S, (g) C. (h) FESEM image of the surface of a WS_2@C-PP separator and (i) blank PP separator. (j) Cross-sectional SEM image of the WS_2@C-PP separator.

structure of 3D flower-like nanospheres with an diameter of 700 ± 300 nm. After the dopamine coating and annealing procedure, no apparent aggregation can be observed, and the WS_2@C composite keeps the morphology of the rough nanosphere whose diameter reaches 1100 ± 300 nm (Figure 2b and c). Figure 2d presents energy dispersive X-ray (EDX) analysis showing the dispersion of W, S, and C over the nanospheres (Figure 2e–g). Besides, Figure 2g indicates that the carbon layer was successively coated on the WS_2 nanospheres and dispersed uniformly (Figure 2e–g). After pasting, the WS_2@C-PP separator remains a superb porous structure comparing with the pure PP separator (Figure 2h and i), which is favorable for the transfer of ions and brings about a higher electrolyte intake.[57] Obviously, the WS_2@C nanospheres keep the more uniform dispersions in comparison with the single WS_2 coating of the PP separator (Figure S1). Besides, the cross-sectional scanning electron microscopy (SEM) image confirms that the WS_2@C-PP separator owns a uniform layer thickness of about 7.5 μm (Figure 2j).

The composition and crystal structure of the products were assessed by X-ray diffraction (XRD) and Raman spectroscopy. According to Figure 3a, the WS_2 and WS_2@C exhibit sharp reflexes at 2θ of 14.0°, 28.2°, 32.7°, 33.5°, 39.5°, and 58.4°, corresponding to pure WS_2 (PDF#08-0237). Also, a small peak at 2θ = 23.5° in the WS_2@C can be indexed to the amorphous carbon phase showing good graphitization, which ensures effective hindrance to LiPSs' diffusion and facilitation of charge transfer. As shown in the Raman spectrum in Figure 3b, the small peaks at 691.1 and 805.5 cm^{-1} are both assigned to W–O–W bonding, indicating slight oxidation of the sample's surface. Meanwhile, the WS_2@C displays a typical D band and G bands at nearly 1346.4 and 1589.1 cm^{-1}, corresponding to lattice defects and sp^2-bonded carbon atoms in graphite, respectively. The intensity ratio of the D and G bands (I_D/I_G) of the WS_2@C (0.86) is far less than that of the pure carbon (1.01), illustrating the high degree of graphitization, which is consistent with the XRD analysis. The highly graphitized carbon layers facilitate electron transport.[58,59]

The surface chemical composition of the WS_2@C composite was examined by X-ray photoelectron spectroscopy (XPS). The survey spectrum in Figure S2a shows the distinct signals of C, N, O, W and S elements. The high-resolution C 1s spectrum shows four peaks (Figure 4a). The peaks at 284.5, 285.2 eV correspond to the C–C, C–N bonds, and the peaks at 286.1, 289.1 eV are assigned to the C–O, O–C=O bonds. The existing peak of C–N is attributed to the presence of N-doping in the carbon lattice. The oxygen groups existing on the surface are considered to augment the binding power to LiPSs.[14] The N 1s spectrum is shown in Figure 4b. The peaks at 399.1, 400.3, and 401.0 eV can be ascribed to three nitrogen's chemical states, namely the pyridinic N (N-6), pyrrolic N (N-5), and graphitic N (N–G),[60] respectively, derived from dopamine-HCl. Among them, the appearance of N-5, N-6 with super electronegativity result in the stronger adsorptive ability of LiPSs, compared to a pure carbon matrix.[61,62] The W 4f spectrum (Figure 4c) is fitted by three characteristic peaks of W^{4+}, ascribed to W $4f_{7/2}$ (32.6 eV), W $4f_{5/2}$ (34.8 eV) and W $5p_{3/2}$ (38.1 eV). Besides, the peaks at 35.5, 37.7 and 41.0 eV are assigned to W $4f_{7/2}$, W $4f_{5/2}$ and W $5p_{3/2}$ of W^{6+}, respectively, verifying a slight oxidation of the WS_2's surface again.[63,64] In the S 2p spectrum (Figure 4d), the peaks at 162.3, 163.5 eV, belong to S $2p_{3/2}$, S $2p_{1/2}$ of sulfidic nature. The O 1s peaks in Figure S2b were deconvoluted into 4 peaks at 530.7, 531.9, 532.7 and 533.9 eV, which can be assigned to oxygen in the W–O–W bonds, W–O–H bonds, C–O bonds, and the surface adsorption H_2O, corresponding to the presence of the surface oxidation state.[37]

With the macroporous structure, the commercial PP separator allows LiPSs to pass through easily, causing detrimental shuttle effects. Coating the WS_2@C layer onto the surface of PP is believed to effectively solve this problem. To verify the strong adsorption ability to the long-chain LiPSs, an H-shaped permeating test was performed for visualization. The dark Li_2S_6 solution (50 mL, 10 mmol L^{-1}) and the apparent 1,2-dimethoxyethane (DME) and 1,3-dioxolane (DOL) mixed solution with a volume ratio of 1 : 1 were separated by the PP (Figure S3a), C-PP (Figure S3b), WS_2-PP (Figure S3c), and WS_2@C-PP (Figure S3d)

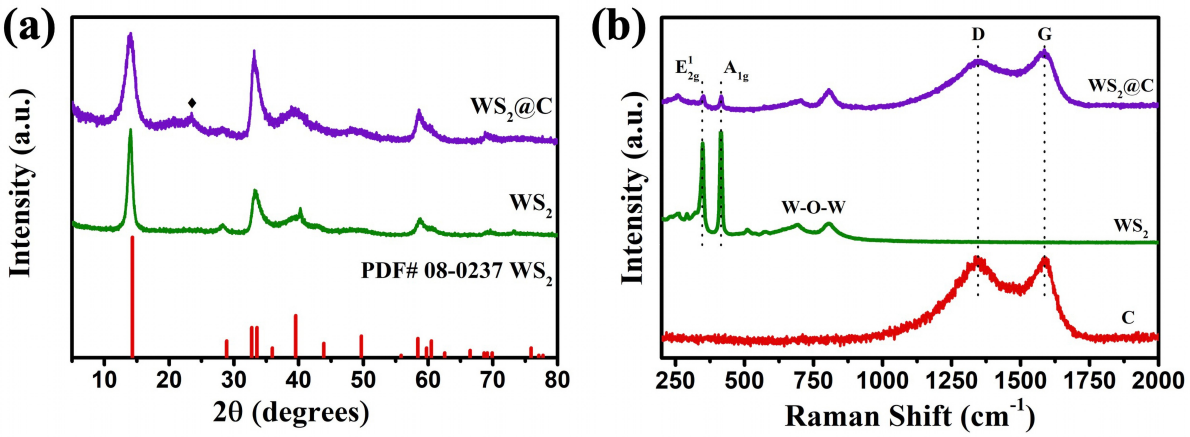

Figure 3. (a) XRD patterns of WS_2@C and WS_2. (b) Raman spectra of C, WS_2, and WS_2@C.

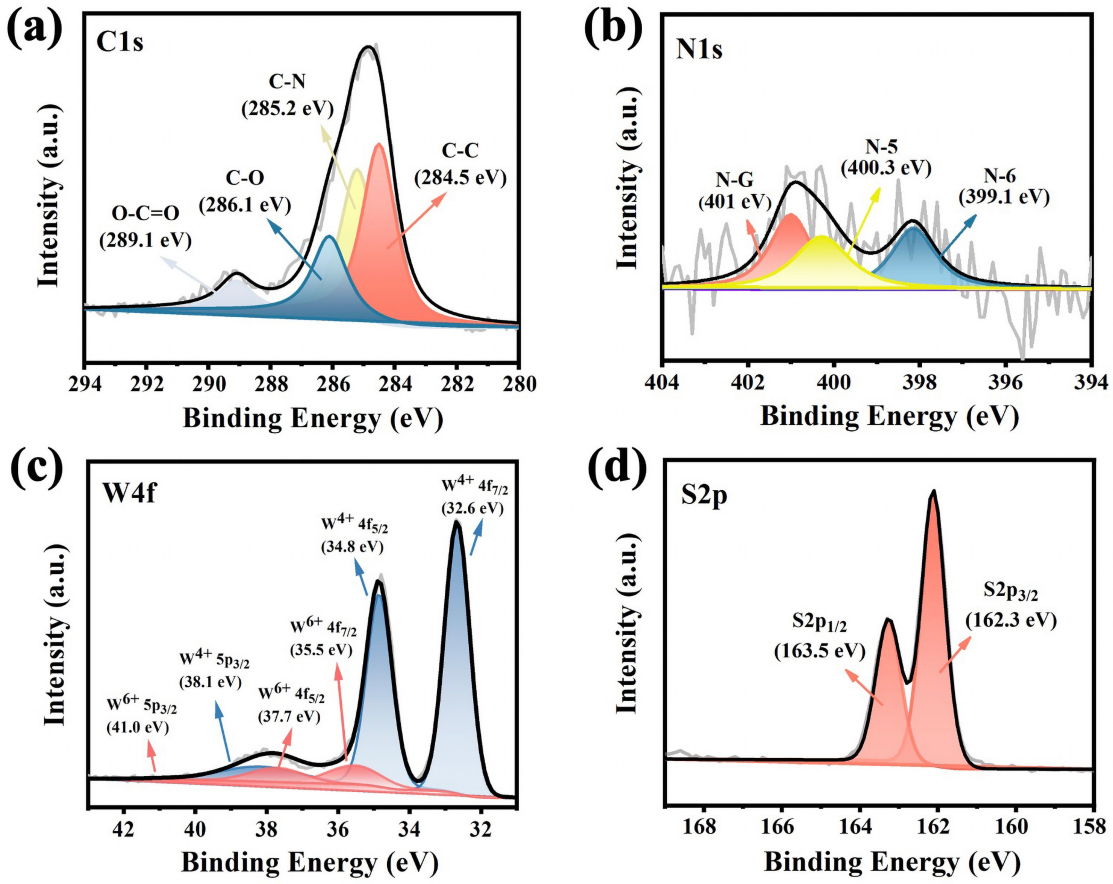

Figure 4. XPS region spectra of (a) C 1s, (b) N 1s, (c) W 4f, (d) S 2p of WS_2@C.

separators. In Figure S3a, the blank PP separator failed to prevent Li_2S_6 diffusion as the color of the right side gradually changed to deep yellow only after half an hour. After 12 h, the electrolyte separated by C-PP (Figure S3b) and WS_2-PP (Figure S3c) separators exhibited a slight change to light yellow, demonstrating a certain ability to alleviate the shuttle effects. In contrast, the color of the device with the WS_2@C-PP separator (Figure S3d) stayed almost transparent after 12 h, proving great interaction with LiPSs and restriction to the shuttle effects. The corresponding ultraviolet-visible (UV-vis) spectra (Figure S4) shows the relatively lowest absorbance for the solution permeating through the WS_2@C-PP separator, in the 400–500 nm region where the strong absorption peak for fresh polysulfide solution would be observed,[65,66] furtherly proving the superb restriction of WS_2@C to the shuttle of LiPSs. Additionally, the S 2p spectrum of the WS_2@C-PP/Li_2S_6 (Figure S5b) shows various sulfur environments. Apart from the two peaks [BE ($S2p_{3/2}$) = 162.3 eV, BE ($S2p_{1/2}$) = 163.5 eV] belonging to the pristine WS_2, another doublet at BE ($S2p_{3/2}$) = 168.2 eV and BE ($S2p_{1/2}$) = 169.7 eV appears. Those are assigned to the presence of sulfates, arising from a surface redox reaction between Li_2S_6 and WS_2, plus the further reactions, which would bind LiPSs chemically and catalyze the conversion from long-chain polysulfides to short-chain one.[45,67]

To further evaluate the performance of the modified separator, its mechanical properties and wettability are systematically investigated. The wettability of four different separators is displayed in Figure S6. The contact angle of the bare PP separator towards the electrolyte was up to 49.3°, while that of the C-PP and WS_2-PP separators were 9.8° and 8°. As for the WS_2@C-PP separator, the value was the smallest one (7.5°), indicating that it could increase the surface wettability and accelerate the electrolyte to soak.[68] This feature benefits the compatibility of the electrode-separator interface, plus helping to maintain the electrolyte in the separator, which could improve the transport of ions through the separator.[69] Figure S7 shows horizontal (a) and vertical (b) tensile stress-strain curves of the different separators. The WS_2@C-PP separator owns the highest tensile strength with a horizontal tensile strength of 27.52 MPa (Figure S7a) and a vertical tensile strength of 275.35 MPa (Figure S7b), much stronger than that of the PP separator (23.87 MPa, 255.72 MPa) alone. Therefore, the WS_2@C-PP separator could efficiently protect the cells against the formation of Li dendrites by its mechanical strength.[69]

Electrochemical Performance

The electrochemical performances of the PP, WS_2-PP, C-PP, and WS_2@C-PP separators were tested with CR2016 coin-type cells consisting of sulfur-Al cathode and metallic lithium anode. The first three cyclic voltammetry (CV) curves of the WS_2@C-PP separator are shown in Figure 5a, with two cathodic peaks and an anodic peak. Generally, the two cathodic peaks at around 2.34 and 2.00 V vs. Li/Li^+ are ascribed to the conversion of elemental sulfur (S_8) to high-order soluble LiPSs, and subsequent formation of the disulfide or monosulfide (Li_2S_2/Li_2S); the anodic peak occurring at about 2.39 V is attributed to the transformation from insoluble Li_2S_2/Li_2S to sulfur. Compared with the first anodic scan, the oxidation peak of the second scan witnesses an obvious shift, because of the rearrangement of the migrating polysulfides to an electrochemical state that is close to that of elemental sulfur.[56,70] Besides, the two CV curves of the 2nd and 3rd scan conform with each other, which shows electrochemical cycling stability and reversibility of the separator. We then measured the electrochemical kinetics of the cells with different separators by electrochemical impedance spectroscopy (EIS) (Figure 5b). All Nyquist plots exhibit a straight line in the low-frequency region and a compressed semicircle in the high-middle frequency region. The EIS spectra of the batteries with four different separators are modeled with equivalent circuits (Figure 5b). Table S1 displays the results, and the WS_2@C-PP has the considerably lowest R_{ct} (charge transfer resistance) of 75.7 Ω, much lower than that of the pure PP separator (189.7 Ω). This fact reveals the fast ion diffusion as well as the improved transfer rate of charge among the interface of the electrode, separator, and electrolyte.

The rate performances of the Li-S batteries with the bare PP, C-PP, WS_2-PP, and WS_2@C-PP separators were evaluated by galvanostatic charge/discharge at different current densities (0.1, 0.2, 0.5, 1, and 2 C) (Figure 6a). With the WS_2@C-PP separator, the cell delivers initial discharge capacities of 1376, 851, 698, 567, and 446 mAh g^{-1}, respectively, which are much higher than those of the batteries with other separators. Also, when the discharge rate goes back to 0.5 C, the specific capacity still retains 687 mAh g^{-1}, equal to around 98.4% of the original capacity, demonstrating excellent redox kinetics, outstanding electron/ion transport properties, and highly reversible electrochemistry. Figure 6b exhibits the galvanostatic charge/discharge curves in the first cycle at 0.1 C. It can be observed that there are three distinct platforms in the profiles of the WS_2@C-PP separator, including two in the discharge profiles, conforming to its CV curves. Visibly, the overpotential ($\triangle E$), between charge/discharge curves, mainly relates to the electrochemical reaction kinetics.[15] Consequently, the modified separators, especially the WS_2@C-PP separator, possess lower polarizations and better redox conversion to LiPSs. The long-term cycling performances at 0.1 C are compared in Figure 6c. The huge drop in capacity in the first 50 cycles may be due to irreversible loss of capacity when some LiPSs dissolves (this is particularly noticeable at high current densities), or because the sulfur in the cathode was not activated enough in the first several cycles. Particularly, owing to the fast electron/ion diffusion and high-efficiency suppression to LiPSs, the WS_2@C-PP separator exhibits the highest initial discharge capacity (1475 mAh g^{-1}). After 300 cycles, the discharge capacity is maintained at 662 mAh g^{-1}, with a stable Coulombic efficiency (approximately 100%). For comparison, cells with bare PP, C-PP, and WS_2-PP separators only have 238, 440, and 497 mAh g^{-1} left, respectively. The best cycling stability of the WS_2@C-PP separator suggests the prominent ability of reutilizing active materials and alleviating volume expansion, resulting from its abundant physically/chemically active sites with LiPSs. The charge/discharge profiles in the first cycle of the WS_2@C-PP separator at 0.1, 0.2, 0.5, 1, and 2 C are shown in Figure 6d. With the increasing current, the overpotential gets to expand, while the charge/discharge plateau is still well-defined, conforming to the exceptional redox kinetics of LiPSs again. Besides, a long-term cycle test is carried out at 1 C to further investigate its application potential (Figure 6e). At first, when the cell experiences an activation at 0.1 C, its discharge capacity goes up to 1234 mAh g^{-1}. When the current amplifies to 1 C sharply, a

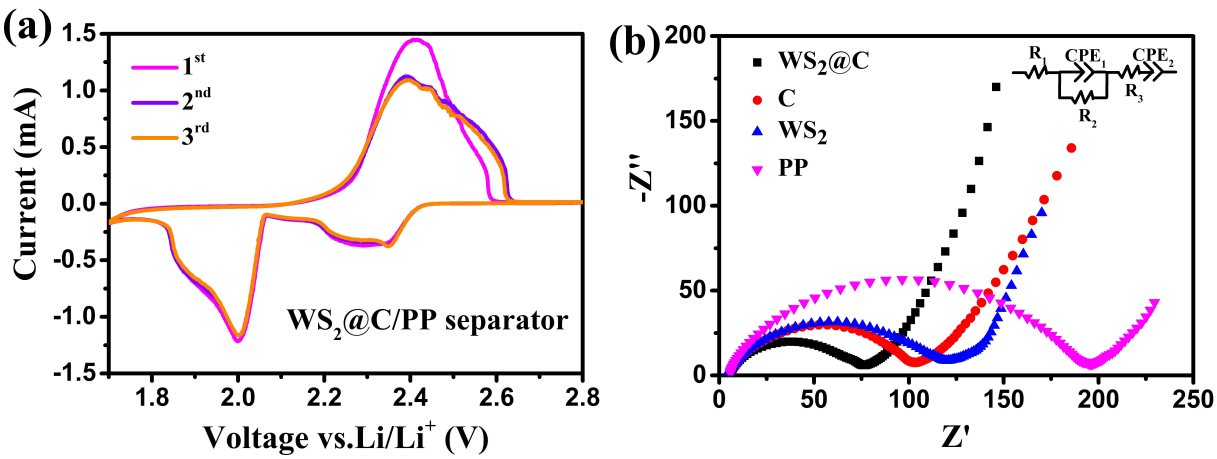

Figure 5. (a) CV curves of symmetric cells with the WS_2@C-PP separator at a scan rate of 0.1 mV s^{-1}. (b) Nyquist plots of PP, WS_2, WS_2@C, WS_2@C-PP separators, and the inset exhibits the equivalent circuit for simulating the electrochemical models of the Li-S batteries.

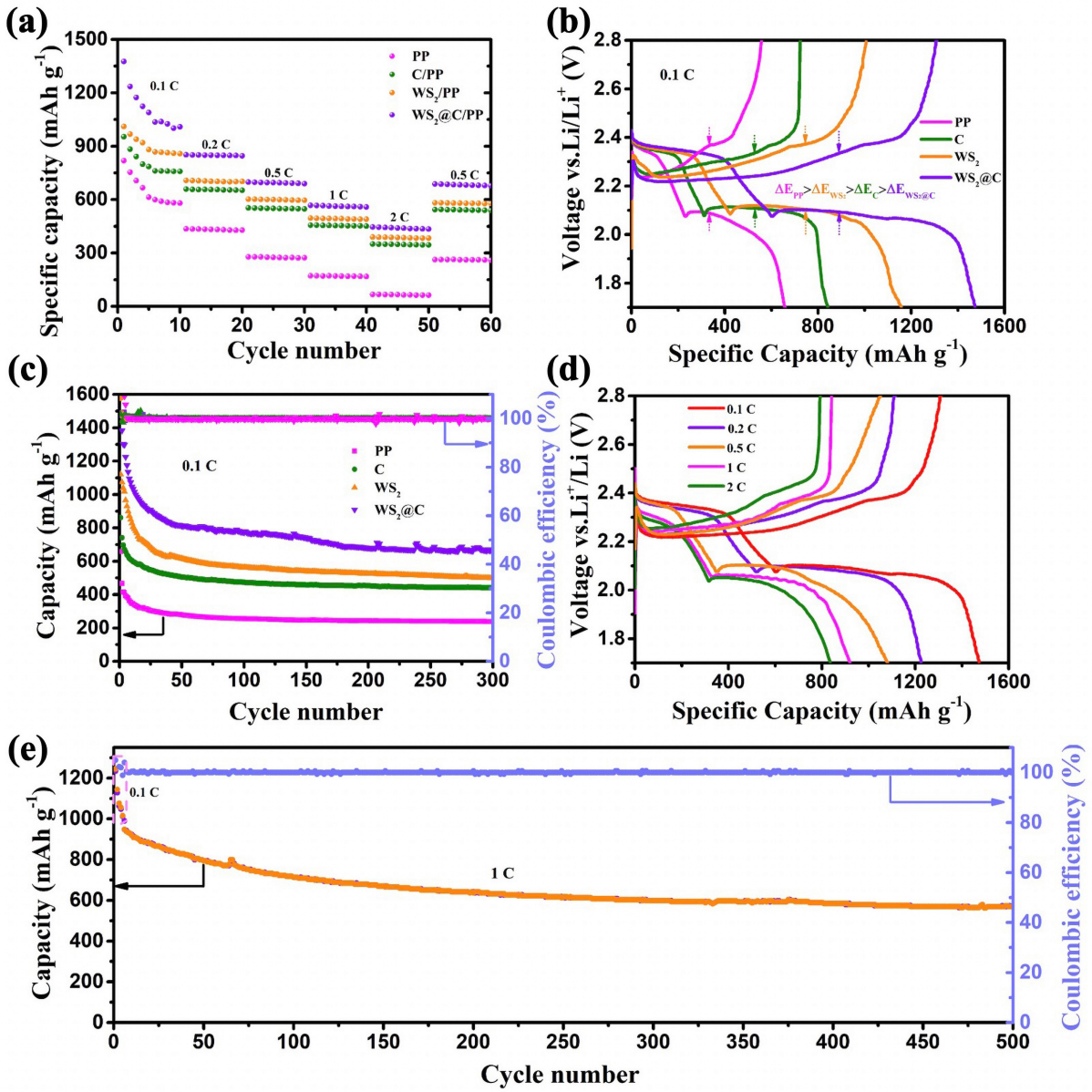

Figure 6. Electrochemical performances of Li-S batteries. (a) Rate performance of the cells with various separators at diverse C-rates from 0.1 C to 2 C. (b) Charge-discharge profiles of the cells with PP, C-PP, WS_2-PP, WS_2@C-PP separators at 0.1 C rate. (c) Cycling performance at a rate of 0.1 C over 300 cycles with the above four kinds of separators. (d) Charge-discharge profiles in the first circle of the WS_2@C-PP at different current densities. (e) Long cycling performance of the WS_2@C-PP separator at 1 C.

noticeable capacity drop can be found, and an initial capacity of 943 mAh g^{-1} is realized. Over 500 cycles, the capacity of the cell slowly reduces to 569 mAh g^{-1} with a fading rate as slow as 0.07% per cycle. In the meantime, the corresponding Coulombic efficiency maintains approximately 99% all the time. These results are better than many reported modified separators (Table S2), delivering the WS_2@C-PP separator with an outstanding rate capacity and cyclic stability.

To further test the stability of the WS_2@C coating, the modified separator and C-PP based cells were examined after 100 cycles at 0.1 C, followed by being disassembled at the same fully discharge status. As shown in Figure S8, the cycled WS_2@C-PP separator has an intact and compact surface (Figure S8a), whereas obvious cracks can be detected on the C-PP separator surface (Figure S8b). These results point to the improved long-term stability of the WS_2@C coating. Also, the corresponding EDX mapping of WS_2@C-PP (Figure S8c) displays a consistent distribution of both carbon and sulfur signals with no evidence for agglomerated sulfur-related species, corroborating the catalytic properties of WS_2 in promoting LiPSs' conversion.[2,3]

The XPS data in Figure S9 shows the chemical composition of the WS_2@C-PP separator before and after cycling at different currents (0.1 C and 2 C). The W 4f spectrum is shown in Figure S9a. The peaks at 32.6, 34.8, and 38.1 eV are attributed to WS_2, and the small peaks at 35.5, 37.7, and 41.0 eV are assigned to WO_3. After cycling, the W^{6+} doublet peaks increase, assigned

to a more pronounced presence of WO_3 which is probably generated from the redox reaction of polysulfide and electrolyte during cycling. When the cycling current increases, there is not enough time for polysulphide to be catalytically converted by WS_2, so the degree of oxidation on the surface of WS_2 is further increased. Moreover, the peaks of W $4f_{7/2}$ and W $4f_{5/2}$ shift to lower binding energies ($\Delta E = 0.28$ and 0.2 eV, respectively) after cycling, which further indicates a strong interaction of WS_2 with polysulfide, demonstrating that WS_2 anchors the LiPSs as well as facilitates their conversion and thereby ameliorates their accumulation. Figure S9b shows the S2p spectrum before and after cycling. The doublet peaks at 162.3 and 163.5 eV are attributed to S^{2-} in WS_2. After cycling, strong doublet peaks at 168.5 and 169.7 eV appear relating to the presence of sulfates, which can act as mediators to bind polysulfide species and convert them to lower-order polysulfides during discharge.

From the above experimental data, we can suggest a possible mechanism of the WS_2@C-PP separator enhancing Li-S battery properties as follows: when the Li-S battery is discharged, S_8 in the cathode will turn into Li_2S_6 and Li_2S_4, which are soluble in the electrolyte.[71,72] In this process, the WS_2 nanostructures' surface-active sites in the WS_2@C-PP separator will moderately adsorb the above LiPSs through S–W bonds formed by electrostatic interaction, so that the LiPSs get trapped on the sulfophilic sites instead of diffusing to the anode side. Meanwhile, the high electrical conductivity of the present carbon materials can facilitate charge transfer at the interface of WS_2@C and LiPSs, thereby catalyzing conversion reactions from soluble long-chain (Li_2S_6 and Li_2S_4) to insoluble short-chain LiPSs (Li_2S_2 and Li_2S) in cathode side. Finally, the WS_2@C-PP separator successfully depresses shuttle effects and prevents loss of active materials in the Li-S battery, contributing to an improved capacity than pure PP does.

Conclusion

In summary, we have built an advanced modified PP-separator coated with flower-like WS_2@C nanospheres consisting of 2D WS_2 nanosheets and carbon layers. Owing to the merits of each component, the WS_2@C-PP separator owns high conductivity, adsorptive and electrocatalytic ability towards LiPSs, effectively suppressing the shuttle effects, while promoting the reutilization of active material. The novel morphology of the carbon-coated WS_2 nanoflowers makes the best use of the above synergistic effects, as well as contributes to their uniform dispersion on the PP separator. Besides, the modified separator possesses enhanced mechanical properties and electrolyte wettability. Therefore, the Li-S cell with the WS_2@C-PP separator displays outstanding cycling stability and rate performances. When it cycles at 0.1 C, the discharge capacity reaches 1475 mAh g^{-1} and it provides 943 mAh g^{-1} initially at 1 C, with a sluggish decay rate of only 0.07 % after 500 cycles. Our results highlight a facile design of functional separators for Li-S batteries and help in addressing issues currently hampering their commercial implementation.

Experimental Section

Chemicals

Tungsten hexachloride (WCl_6) and Tris were purchased from Maclin. Thioacetamide (C_2H_5NS), dopamine hydrochloride (dopamine-HCl), sulfur sublimed, lithium disulfide (Li_2S), 1,2-dimethoxyethane (DME), 1,3-dioxolane (DOL) were purchased from Aladdin. All reagents were analytical grade and used without further purification. The polyvinylidene difluoride (PVDF), N-methyl-2-pyrrolidone (NMP), Super P Li, Al foil, and metallic lithium for making electrodes all were battery grade. Deionized water was produced from an ultrapure water system (Heal Force, Hong Kong) and used throughout the whole experiment.

Preparation of WS_2

Firstly, 0.991 g WCl_6 and 1.878 g C_2H_5NS were dissolved in 50 mL of deionized water with an ultrasonic dispersion to mix the solution thoroughly. After that, the solution was subjected to a hydrothermal reaction at 240 °C for one day. After collecting, the precipitate was washed by centrifugation (10000 rpm, 10 min) with deionized water and ethanol several times. Lastly, the black WS_2 powder was obtained through drying at 60 °C under vacuum conditions for 12 h.

Preparation of WS_2@C

200 mg dopamine-HCl was dissolved in 200 mL of freshly prepared Tris buffer solution (0.05 M, pH 8.5). Subsequently, 200 mg WS_2 were added to the above solution and stirred for one day. After that, the product was washed completely with deionized water and ethanol several times and dried at 60 °C for 12 h. The WS_2@C composite was gained after annealing in a tube oven at 600 °C for 6 h in an argon atmosphere with a heating rate of 5 °C min^{-1}. Besides, a comparison sample was made through similar steps without adding WS_2, denoted as C composite.

Preparation of WS_2@C-PP and C-PP Separators

To form a homogeneous slurry, 320 mg as-prepared WS_2@C and 80 mg PVDF were blended in 2 mL NMP. Next, the WS_2@C-PP separator was obtained after pasting the slurry onto a PP separator (Celgard 2400) and dried at 40 °C for 3 h in the vacuum condition. Then, the obtained membrane was cut into the needed disk-shaped slices. The C-PP separator was also fabricated by the same approach.

Preparation of Li_2S_6 Solution

The LiPSs (Li_2S_6) solution was synthesized to simulate the electrolyte based on the former literature.[73] Initially, Li_2S and sulfur in a molar ratio of 1:5 were added into a mixed solution containing the same volume of DME and DOL. Then a dark orange 0.2 M Li_2S_6 solution was obtained after stirring for 2 days. Importantly, the above process was carried out in an argon gas-filled glove box.

Fabrication of Sulfur-Al Cathode

To assemble the sulfur-Al cathode, Sulfur, Super P, and PVDF were mixed with a mass ratio of 7:2:1 in NMP (C_5H_9NO) to obtain a slurry. Then, the slurry was pasted onto Al foil current collectors of 1.43 mg cm^{-2} and dried at 60 °C for 12 h in a vacuum. The dried Al

foil was lastly cut into small disks to obtain positive electrodes. Each cathode possessed 1.0 mg cm^{-2} of sulfur.

Materials Characterization

The element distribution, morphology, and microstructure of the products were observed by a sigma-500 FESEM equipped with EDX mapping. XRD patterns were collected with a Bruker D8 ADVANCE diffractometer with Cu Kα radiation from $2\theta = 5°$ to 80° for measuring the crystal structures. Elemental surface composition and chemical state information were obtained by XPS on a Thermo Fisher Escalab 250Xiinstrument, with binding energy calibration using the C 1s peak of adventitious (284.5 eV) as a reference. Raman spectra were recorded on a LabRAM HR 800UV with an excitation laser of 532 nm. UV-vis absorption spectra were gained on a UV-3600 plus spectrometer single beam instrument over a range of 350–700 nm. The contact angles were measured by a JC2000DB instrument (China). The tensile strength of the separators was tested by a dynamic mechanical analysis machine in tension mode.

Battery Assembly and Electrochemical Measurements

To prepare the electrolyte, 1 M LiTFSI was added into a mixed solution of DME and DOL (v/v = 1/1) with 1 wt% $LiNO_3$ which acted as the additive, to suppress the shuttle of soluble LiPSs on the anode. Following the previous literature,[74–76] the electrolyte addition was controlled at an E/S ratio of 10 mL g^{-1}. Coin-type (CR2016) cells were assembled with the modified separators, sulfur-Al cathode, and metallic lithium anode in an argon-filled glove box. At various current densities, galvanostatic charge-discharge tests were carried out from 1.7 to 2.8 V (vs. Li^+/Li) by a Land battery test system. A multi-channel Autolab electrochemical workstation (M204, Netherlands) was used to record CV at a scan rate of 0.1 mV s^{-1} in the potential range of 1.7–2.8 V. EIS data was collected with an electrochemical workstation (Shanghai Chenhua Co. Ltd., CHI 760E, China) at frequencies ranging between 10 MHz and 100 kHz. All the above measurements were conducted at room temperature.

Acknowledgements

This work was supported by the Ministry of Science and Technology of China [grant number 2016YFA0200200]; the National Natural Science Fund of China [grant numbers 51673060, 11574075]; and the China Scholarship Council. Open Access funding enabled and organized by Projekt DEAL.

Conflict of Interest

The authors declare no conflict of interest.

Data Availability Statement

The data that support the findings of this study are available from the corresponding author upon reasonable request.

Keywords: catalyzation · flower-like structure · lithium-sulfur battery · synergistic effect · WS_2 nanosheets

[1] B. Dunn, H. Kamath, J.-M. Tarascon, *Science* **2011**, *334*, 928–935.
[2] J. Balach, T. Jaumann, M. Klose, S. Oswald, J. Eckert, L. Giebeler, *Adv. Funct. Mater.* **2015**, *25*, 5285–5291.
[3] J. Xu, W. Zhang, H. Fan, F. Cheng, D. Su, G. Wang, *Nano Energy* **2018**, *51*, 73–82.
[4] G. Xu, A. Kushima, J. Yuan, H. Dou, W. Xue, X. Zhang, X. Yan, J. Li, *Energy Environ. Sci.* **2017**, *10*, 2544–2551.
[5] Y. Tsao, M. Lee, E. C. Miller, G. Gao, J. Park, S. Chen, T. Katsumata, H. Tran, L.-W. Wang, M. F. Toney, Y. Cui, Z. Bao, *Joule* **2019**, *3*, 872–884.
[6] J. Chang, J. Shang, Y. Sun, L. K. Ono, D. Wang, Z. Ma, Q. Huang, D. Chen, G. Liu, Y. Cui, Y. Qi, Z. Zheng, *Nat. Commun.* **2018**, *9*, 4480.
[7] Q. Pang, A. Shyamsunder, B. Narayanan, C. Y. Kwok, L. A. Curtiss, L. F. Nazar, *Nat. Energy* **2018**, *3*, 783–791.
[8] L. Carbone, T. Coneglian, M. Gobet, S. Munoz, M. Devany, S. Greenbaum, J. Hassoun, *J. Power Sources* **2018**, *377*, 26–35.
[9] F. Ma, Y. Wan, X. Wang, X. Wang, J. Liang, Z. Miao, T. Wang, C. Ma, G. Lu, J. Han, Y. Huang, Q. Li, *ACS Nano* **2020**, *14*, 10115–10126.
[10] X.-B. Cheng, R. Zhang, C.-Z. Zhao, Q. Zhang, *Chem. Rev.* **2017**, *117*, 10403–10473.
[11] D. Lin, Y. Liu, Y. Cui, *Nat. Nanotechnol.* **2017**, *12*, 194–206.
[12] S.-F. Ng, M. Y. L. Lau, W.-J. Ong, *Adv. Mater.* **2021**, *33*, 2008654.
[13] N. Jayaprakash, J. Shen, S. S. Moganty, A. Corona, L. A. Archer, *Angew. Chem. Int. Ed.* **2011**, *50*, 5904–5908; *Angew. Chem.* **2011**, *123*, 6026–6030.
[14] S. Y. Zheng, Y. Chen, Y. H. Xu, F. Yi, Y. J. Zhu, Y. H. Liu, J. H. Yang, C. S. Wang, *ACS Nano* **2013**, *7*, 10995–11003.
[15] S. Zhou, J. Liu, F. Xie, Y. Zhao, T. Mei, Z. Wang, X. Wang, *J. Mater. Chem. A* **2020**, *8*, 11327–11336.
[16] G. Gao, X. Sun, L.-W. Wang, *J. Mater. Chem. A* **2020**, *8*, 21711–21720.
[17] G. Hu, C. Xu, Z. Sun, S. Wang, H.-M. Cheng, F. Li, W. Ren, *Adv. Mater.* **2016**, *28*, 1603–1609.
[18] P. Shi, T. Li, R. Zhang, X. Shen, X.-B. Cheng, R. Xu, J.-Q. Huang, X.-R. Chen, H. Liu, Q. Zhang, *Adv. Mater.* **2019**, *31*, 1807131.
[19] F. Pei, A. Fu, W. Ye, J. Peng, X. Fang, M.-S. Wang, N. Zheng, *ACS Nano* **2019**, *13*, 8337–8346.
[20] J. Liu, L. Yuan, K. Yuan, Z. Li, Z. Hao, J. Xiang, Y. Huang, *Nanoscale* **2016**, *8*, 13638–13645.
[21] A. Paolella, H. Demers, P. Chevallier, C. Gagnon, G. Girard, N. Delaporte, W. Zhu, A. Vijh, A. Guerfi, K. Zaghib, *J. Power Sources* **2019**, *427*, 201–206.
[22] Z. A. Ghazi, X. He, A. M. Khattak, N. A. Khan, B. Liang, A. Iqbal, J. Wang, H. Sin, L. Li, Z. Tang, *Adv. Mater.* **2017**, *29*, 1606817.
[23] H.-J. Peng, J.-Q. Huang, X.-B. Cheng, Q. Zhang, *Adv. Energy Mater.* **2017**, *7*, 1700260.
[24] S. Bai, X. Liu, K. Zhu, S. Wu, H. Zhou, *Nat. Energy* **2016**, *1*, 16094.
[25] J. Li, Z. Xiao, A. Chen, W. Zhang, D. Zhu, Y. Jin, Q. Mao, G. Wang, J. He, Y. Xia, *Front. Energy Res.* **2020**, *8*, 593640.
[26] S.-H. Chung, A. Manthiram, *Adv. Funct. Mater.* **2014**, *24*, 5299–5306.
[27] J.-Q. Huang, T.-Z. Zhuang, Q. Zhang, H.-J. Peng, C.-M. Chen, F. Wei, *ACS Nano* **2015**, *9*, 3002–3011.
[28] P. Zeng, L. Huang, X. Zhang, R. Zhang, L. Wu, Y. Chen, *Chem. Eng. J.* **2018**, *349*, 327–337.
[29] Q. Li, Y. Liu, L. Yang, Y. Wang, Y. Liu, Y. Chen, X. Guo, Z. Wu, B. Zhong, *J. Colloid Interface Sci.* **2021**, *585*, 43–50.
[30] J.-Q. Huang, Q. Zhang, H.-J. Peng, X.-Y. Liu, W.-Z. Qian, F. Wei, *Energy Environ. Sci.* **2014**, *7*, 347–353.
[31] F. Pei, L. L. Lin, A. Fu, S. G. Mo, D. H. Ou, X. L. Fang, N. F. Zheng, *Joule* **2018**, *2*, 323–336.
[32] Y. Li, J. Qian, M. Zhang, S. Wang, Z. Wang, M. Li, Y. Bai, Q. An, H. Xu, F. Wu, L. Mai, C. Wu, *Adv. Mater.* **2020**, *32*, 2005802.
[33] Y. Wang, D. Kong, W. Shi, B. Liu, G. J. Sim, Q. Ge, H. Y. Yang, *Adv. Energy Mater.* **2016**, *6*, 1601057.
[34] S.-J. Kim, K. Kim, J. Park, Y.-E. Sung, *ChemCatChem* **2019**, *11*, 2373–2387.
[35] T. Lei, W. Chen, J. Huang, C. Yan, H. Sun, C. Wang, W. Zhang, Y. Li, J. Xiong, *Adv. Energy Mater.* **2017**, *7*, 1601843.
[36] Q. F. Zhang, Y. P. Wang, Z. W. Seh, Z. H. Fu, R. F. Zhang, Y. Cui, *Nano Lett.* **2015**, *15*, 3780–3786.
[37] M. Xiong, J. Qian, K. Yang, Z. Chen, T. Mei, J. Wang, J. Li, L. Yu, X. Wang, *J. Mater. Sci.* **2020**, *55*, 12031–12040.

[38] B. Zhang, C. Luo, Y. Deng, Z. Huang, G. Zhou, W. Lv, Y.-B. He, Y. Wan, F. Kang, Q.-H. Yang, *Adv. Energy Mater.* **2020**, *10*, 2000091.
[39] X. Chen, H.-J. Peng, R. Zhang, T.-Z. Hou, J.-Q. Huang, B. Li, Q. Zhang, *ACS Energy Lett.* **2017**, *2*, 795–801.
[40] J. Park, B. C. Yu, J. S. Park, J. W. Choi, C. Kim, Y. E. Sung, J. B. Goodenough, *Adv. Energy Mater.* **2017**, *7*, 1602567.
[41] H. G. Füchtbauer, A. K. Tuxen, P. G. Moses, H. Topsøe, F. Besenbacher, J. V. Lauritsen, *Phys. Chem. Chem. Phys.* **2013**, *15*, 15971–15980.
[42] T. Li, X. Bai, U. Gulzar, Y.-J. Bai, C. Capiglia, W. Deng, X. Zhou, Z. Liu, Z. Feng, R. Proietti Zaccaria, *Adv. Funct. Mater.* **2019**, *29*, 1901730.
[43] K. Shiva, H. Matte, H. B. Rajendra, A. J. Bhattacharyya, C. N. R. Rao, *Nano Energy* **2013**, *2*, 787–793.
[44] S. Xiao, J. Zhang, Y. Deng, G. Zhou, R. Wang, Y.-B. He, W. Lv, Q.-H. Yang, *ACS Appl. Energ. Mater.* **2020**, *3*, 4923–4930.
[45] S. Ali, M. Waqas, X. Jing, N. Chen, D. Chen, J. Xiong, W. He, *ACS Appl. Mater. Interfaces* **2018**, *10*, 39417.
[46] Y. C. Liu, N. Zhang, H. Y. Kang, M. H. Shang, L. F. Jiao, J. Chen, *Chem. Eur. J.* **2015**, *21*, 11878–11884.
[47] J. Q. Zhang, H. Sade, Y. F. Zhao, A. T. Murdock, A. Bendavid, J. P. Lellouche, G. X. Wang, Z. J. Han, *Nanotechnology* **2019**, *30*, 035401.
[48] R. D. Nikam, A. Y. Lu, P. A. Sonawane, U. R. Kumar, K. Yadav, L. J. Li, Y. T. Chen, *ACS Appl. Mater. Interfaces* **2015**, *7*, 23328–23335.
[49] X. Zeng, Z. Ding, C. Ma, L. Wu, J. Liu, L. Chen, D. G. Ivey, W. Wei, *ACS Appl. Mater. Interfaces* **2016**, *8*, 18841–18848.
[50] L. Cheng, W. J. Huang, Q. F. Gong, C. H. Liu, Z. Liu, Y. G. Li, H. J. Dai, *Angew. Chem. Int. Ed.* **2014**, *53*, 7860–7863; *Angew. Chem.* **2014**, *126*, 7994–7997.
[51] X. Shang, K. L. Yan, Z. Z. Liu, S. S. Lu, B. Dong, J. Q. Chi, X. Li, Y. R. Liu, Y. M. Chai, C. G. Liu, *Appl. Surf. Sci.* **2017**, *402*, 120–128.
[52] T. S. Sahu, S. Mitra, *Scientific Rep.* **2015**, *5*. 12571.
[53] T. Li, X. Bai, U. Gulzar, Y.-J. Bai, C. Capiglia, W. Deng, X. Zhou, Z. Liu, Z. Feng, R. Proietti Zaccaria, *Adv. Funct. Mater.* **2019**, *29*, 1901730.
[54] Y. Li, Y. H. Xu, Z. H. Wang, Y. Bai, K. Zhang, R. Q. Dong, Y. N. Gao, Q. Ni, F. Wu, Y. J. Liu, C. A. Wu, *Adv. Energy Mater.* **2018**, *8*, 1800927.
[55] W. T. Koo, J. H. Cha, J. W. Jung, S. J. Choi, J. S. Jang, D. H. Kim, I. D. Kim, *Adv. Funct. Mater.* **2018**, *28*, 1802575.
[56] C.-Y. Fan, S.-Y. Liu, H.-H. Li, Y.-H. Shi, H.-C. Wang, H.-F. Wang, H.-Z. Sun, X.-L. Wu, J.-P. Zhang, *J. Mater. Chem. A* **2017**, *5*, 11255–11262.
[57] J. Zhu, Y. Ge, D. Kim, Y. Lu, C. Chen, M. Jiang, X. Zhang, *Nano Energy* **2016**, *20*, 176–184.
[58] J. H. Zhang, M. Huang, B. J. Xi, K. Mi, A. H. Yuan, S. L. Xiong, *Adv. Energy Mater.* **2018**, *8*, 1701330.
[59] D. L. Fang, Y. L. Wang, C. Qian, X. Z. Liu, X. Wang, S. M. Chen, S. J. Zhang, *Adv. Funct. Mater.* **2019**, *29*, 1900875.
[60] D. D. Cai, S. Q. Wang, P. C. Lian, X. F. Zhu, D. D. Li, W. S. Yang, H. H. Wang, *Electrochim. Acta* **2013**, *90*, 492–497.
[61] X. H. Zeng, Z. P. Ding, C. Ma, L. D. Wu, J. T. Liu, L. B. Chen, D. G. Ivey, W. F. Wei, *ACS Appl. Mater. Interfaces* **2016**, *8*, 18841–18848.
[62] G. M. Zhou, E. Paek, G. S. Hwang, A. Manthiram, *Nat. Commun.* **2015**, *6*, 11.
[63] F. Perrozzi, S. M. Emamjomeh, V. Paolucci, G. Taglieri, L. Ottaviano, C. Cantalini, *Sens. Actuators B* **2017**, *243*, 812–822.
[64] J. W. Qian, Z. J. Peng, Z. G. Shen, Z. Y. Zhao, G. L. Zhang, X. L. Fu, *Sci. Rep.* **2016**, *6*, 25574.
[65] W. Chen, T. Qian, J. Xiong, N. Xu, X. Liu, J. Liu, J. Zhou, X. Shen, T. Yang, Y. Chen, C. Yan, *Adv. Mater.* **2017**, *29*, 1605160.
[66] J. Song, Z. Yu, M. L. Gordin, D. Wang, *Nano Lett.* **2016**, *16*, 864–870.
[67] S. Huang, Y. Wang, J. Hu, Y. V. Lim, D. Kong, Y. Zheng, M. Ding, M. E. Pam, H. Y. Yang, *ACS Nano* **2018**, *12*, 9504–9512.
[68] X. Zuo, M. Zhen, C. Wang, *Nano Res.* **2019**, *12*, 829–836.
[69] Y. Li, S. Lin, D. Wang, T. Gao, J. Song, P. Zhou, Z. Xu, Z. Yang, N. Xiao, S. Guo, *Adv. Mater.* **2020**, *32*, 1906722.
[70] Y. Fu, Y.-S. Su, A. Manthiram, *Angew. Chem. Int. Ed.* **2013**, *52*, 6930–6935; *Angew. Chem.* **2013**, *125*, 7068–7073.
[71] H. Marceau, C.-S. Kim, A. Paolella, S. Ladouceur, M. Lagacé, M. Chaker, A. Vijh, A. Guerfi, C. M. Julien, A. Mauger, M. Armand, P. Hovington, K. Zaghib, *J. Power Sources* **2016**, *319*, 247–254.
[72] W. Zhu, A. Paolella, C. S. Kim, D. Liu, Z. Feng, C. Gagnon, J. Trottier, A. Vijh, A. Guerfi, A. Mauger, C. Mx Julien, M. Armand, K. Zaghib, *Sustain. Energy Fuels* **2017**, *1*, 737–747.
[73] J. Q. Huang, Q. Zhang, H. J. Peng, X. Y. Liu, W. Z. Qian, F. Wei, *Energy Environ. Sci.* **2014**, *7*, 347–353.
[74] P. Zeng, L. W. Huang, X. L. Zhang, R. X. Zhang, L. Wu, Y. G. Chen, *Chem. Eng. J.* **2018**, *349*, 327–337.
[75] C. M. Li, H. Zhang, L. Otaegui, G. Singh, M. Armand, *J. Power Sources* **2016**, *326*, 1–5.
[76] A. Mauger, C. M. Julien, A. Paolella, M. Armand, K. Zaghib, *Mater. Sci. Eng. R* **2018**, *134*, 1–21.

Manuscript received: April 27, 2022
Accepted manuscript online: May 14, 2022